Science Translational Medicine AAAS

T-Type Calcium Channel Blockers That Attenuate Thalamic Burst Firing and Suppress Absence Seizures
Elizabeth Tringham *et al.*
Sci Transl Med **4**, 121ra19 (2012);
DOI: 10.1126/scitranslmed.3003120

Editor's Summary

To Soothe a Seizure

Some epileptic children and adolescents experience "absence" seizures hundreds of times a day. Although apparently mild, these seizures ––so named because they involve a sudden, brief absence of consciousness––can be dangerous if they occur during swimming or driving, for example. Unfortunately, the drugs available for treating such seizures are not completely effective. Tringham *et al*. sought to address this problem by rational drug design.

Although the root cause of such seizures is not known, they are associated with abnormal, highly synchronous neuronal activity in certain brain regions. Voltage-gated ion channels, which have crucial functions in generating and propagating neuronal signals, likely play a key role. Several lines of evidence link one type of ion channel, low voltage –activated T-type calcium channels, to absence seizures. Using the structure of an N-type calcium channel blocker as a starting point, the researchers designed and screened small, focused libraries of compounds in a high-throughput assay that monitored calcium influx via a recombinant T-type channel. Two high-affinity T-type calcium channel blockers, termed Z941 and Z944, were identified; Z944 was highly selective for T-type channels and exhibited a preference for inactivated channels (the likely configuration in hyperexcited neurons). In a rat model of absence epilepsy, both compounds markedly reduced the time spent in seizures and the number of seizures per hour. In contrast to current first-line drugs for treating absence seizures, Z941 and Z944 also reduced the average seizure duration and cycle frequency. Both compounds were well tolerated in rats.

Given its in vitro and in vivo activities, Z944 will progress to phase 1 clinical studies to test its safety in humans. Further studies will be needed to determine whether its marked effects in the rat model of absence epilepsy translate to the more complicated human condition.

Science Translational Medicine (print ISSN 1946-6234; online ISSN 1946-6242) is published weekly, except the last week in December, by the American Association for the Advancement of Science, 1200 New York Avenue NW, Washington, DC 20005.

EPILEPSY

T-Type Calcium Channel Blockers That Attenuate Thalamic Burst Firing and Suppress Absence Seizures

Elizabeth Tringham,[1] Kim L. Powell,[2] Stuart M. Cain,[3] Kristy Kuplast,[1] Janette Mezeyova,[1] Manjula Weerapura,[1] Cyrus Eduljee,[1] Xinpo Jiang,[1] Paula Smith,[1] Jerrie-Lynn Morrison,[1] Nigel C. Jones,[2] Emma Braine,[2] Gil Rind,[2] Molly Fee-Maki,[1] David Parker,[1] Hassan Pajouhesh,[1] Manjeet Parmar,[1] Terence J. O'Brien,[2] Terrance P. Snutch[3]*

Absence seizures are a common seizure type in children with genetic generalized epilepsy and are characterized by a temporary loss of awareness, arrest of physical activity, and accompanying spike-and-wave discharges on an electroencephalogram. They arise from abnormal, hypersynchronous neuronal firing in brain thalamocortical circuits. Currently available therapeutic agents are only partially effective and act on multiple molecular targets, including γ-aminobutyric acid (GABA) transaminase, sodium channels, and calcium (Ca^{2+}) channels. We sought to develop high-affinity T-type specific Ca^{2+} channel antagonists and to assess their efficacy against absence seizures in the Genetic Absence Epilepsy Rats from Strasbourg (GAERS) model. Using a rational drug design strategy that used knowledge from a previous N-type Ca^{2+} channel pharmacophore and a high-throughput fluorometric Ca^{2+} influx assay, we identified the T-type Ca^{2+} channel blockers Z941 and Z944 as candidate agents and showed in thalamic slices that they attenuated burst firing of thalamic reticular nucleus neurons in GAERS. Upon administration to GAERS animals, Z941 and Z944 potently suppressed absence seizures by 85 to 90% via a mechanism distinct from the effects of ethosuximide and valproate, two first-line clinical drugs for absence seizures. The ability of the T-type Ca^{2+} channel antagonists to inhibit absence seizures and to reduce the duration and cycle frequency of spike-and-wave discharges suggests that these agents have a unique mechanism of action on pathological thalamocortical oscillatory activity distinct from current drugs used in clinical practice.

INTRODUCTION

Absence seizures are a common seizure type in children with genetic generalized epilepsies (GGEs). Affected patients experience spontaneous, recurrent nonconvulsive seizures that are associated with hypersynchronous oscillatory burst firing in both the thalamus and the cortex. Although the molecular mechanisms underlying the development of epilepsy are poorly understood, voltage-gated ion channels are likely to be critically involved because they are essential for the initiation and propagation of neuronal firing and hence for seizure generation and maintenance (*1*). A number of currently available drugs for treating epilepsy are thought to act by affecting voltage-gated sodium channels, but certain types of voltage-gated calcium (Ca^{2+}) channels are also involved in the generation of seizure activity (*2*, *3*). In particular, low voltage–activated (LVA) T-type Ca^{2+} channels have been implicated in the pathophysiology of absence seizures (*4*, *5*). Absence seizures are generalized, nonconvulsive seizures characterized by temporary behavioral immobility and unresponsiveness that is accompanied by a distinct pattern of bilateral spike-and-wave discharges (SWDs) on an electroencephalogram (EEG) recording. Absence seizures most commonly affect children and adolescents; these individuals can experience hundreds of seizures per day, which can disrupt learning and affect behavior and motor skills (*6*).

Although multiple Ca^{2+} channel subtypes exist that underlie distinct physiological and pathophysiological functions (*7*), the fine control of transmembrane Ca^{2+} influx in response to membrane depolarization is mediated primarily by the pore-forming α_1 subunit (Ca_V) channel, encoded by a family of 10 Ca_V genes (*8*). These channels can be categorized by the voltages at which they typically activate. The high voltage–activated (HVA) Ca^{2+} channels are $Ca_V1.1$ to $Ca_V1.4$ (L types), $Ca_V2.1$ (P/Q type), $Ca_V2.2$ (N type), and $Ca_V2.3$ (R type); the LVA T-type Ca^{2+} channels are $Ca_V3.1$, $Ca_V3.2$, and $Ca_V3.3$. All three T-type isoforms are expressed in the thalamocortical pathway, albeit differentially in the thalamus and neocortex (*9*). A fundamental feature of absence epilepsy is the abnormal and inappropriate switching of the thalamocortical circuitry from a tonic to oscillatory mode of firing, even during wakefulness (*10*). Although the causes of this pathological switching are uncertain, T-type Ca^{2+} channels in the thalamus and cortex are crucial contributing factors (*11*, *12*). These channels generate low-threshold spikes, leading to both burst firing and oscillatory behaviors (*13*). In addition, T-type Ca^{2+} channels are implicated in the action of certain anti-absence seizure drugs (*14*–*16*).

Several lines of evidence have implicated the $Ca_V3.1$ T-type channel in absence seizures and thalamocortical SWDs (*17*–*19*), as has the $Ca_V3.2$ T-type isoform. In the Genetic Absence Epilepsy Rats from Strasbourg (GAERS) model of absence epilepsy, $Ca_V3.2$ mRNA expression and T-type Ca^{2+} currents are elevated in reticular thalamic nucleus (nRT) neurons (*10*, *20*). Further, a missense mutation in the GAERS $Ca_V3.2$ gene (R1584P) results in a gain of function of $Ca_V3.2$ biophysical properties in a splice variant–specific manner and correlates with seizures in F2 progeny rats produced from double-crossed GAERS and NEC (nonepileptic control) animals (*21*).

In humans, point mutations and/or polymorphisms in both $Ca_V3.1$ and $Ca_V3.2$ channel genes occur in patients with GGEs, including absence seizures (*22*–*26*). In vitro studies on some of these alterations show gain-of-function phenotypes of a more depolarized steady-state inactivation, hyperpolarized voltage dependence of channel activation,

[1]Zalicus Pharmaceuticals Ltd., Suite 301, 2389 Health Sciences Mall, Vancouver, British Columbia V6T 1Z3, Canada. [2]Department of Medicine, Royal Melbourne Hospital, University of Melbourne, 4th Floor, Clinical Sciences Building, Royal Parade, Parkville, Victoria 3050, Australia. [3]Michael Smith Laboratories, University of British Columbia, Room 219, 2185 East Mall, Vancouver, British Columbia V6T 1Z4, Canada.
*To whom correspondence should be addressed. E-mail: snutch@msl.ubc.ca

and/or increased channel plasma membrane expression, all of which would be predicted to lead to neuronal hyperexcitability (*27*–*31*).

Together, the available evidence from animals and humans suggests that both the $Ca_V3.1$ and the $Ca_V3.2$ T-type Ca^{2+} channels play prominent roles in absence epilepsy. Ethosuximide, a first-line drug used to treat patients with absence epilepsy, is widely believed to act by the pan-blockade of T-type Ca^{2+} channels in the millimolar plasma concentration range (*16*). However, ethosuximide also affects other ionic conductances and exhibits side effects in humans, such as drowsiness, ataxia, and blurred vision. Its precise mechanism of action remains unclear with respect to T-type Ca^{2+} channels and to its anti-seizure effects (*14*, *16*). In addition, a recent blinded randomized comparative trial demonstrated that more than 40% of patients continue to have absence seizures despite treatment with ethosuximide (*32*). Here, we therefore aimed to identify small organic, orally available, high-affinity T-type Ca^{2+} channel blockers for treatment of absence seizures.

RESULTS

Rational design T-type blockers identifies Z941 and Z944

The state-dependent inhibition of voltage-gated ion channels has been proposed to be an important mechanism of action for a variety of therapeutic indications (*33*). Antiepileptic drugs such as phenytoin, lamotrigine, and carbamazepine all exhibit high affinity for the open and inactivated channel states (*34*–*36*). During seizure activity, neuronal hyperexcitability may drive channels into the open or inactivated states; therefore, blockers targeting these states would preferentially affect neurons undergoing high-frequency firing while sparing low-frequency firing neurons, wherein channels are predominantly in the closed-state configuration. We designed a fluorescence-based assay capable of rapid high-throughput identification of inactivation state–dependent T-type Ca^{2+} channel blockers using human embryonic kidney (HEK) cells coexpressing the human $Ca_V3.2$ T-type channel ($hCa_V3.2$) and the $K_{ir}2.3$ inward rectifier potassium channel. The normal resting membrane potential (RMP) (V_m) of HEK cells (~−25 to −30 mV) puts T-type Ca^{2+} channels primarily into the inactivated state, and the presence of the coexpressed inward rectifier allows for the manipulation of V_m by varying the extracellular potassium concentration, allowing control of the $Ca_V3.2$ channel state.

We used the piperazine-based compound NP118809 (Z160; Fig. 1A), a high-affinity N-type Ca^{2+} channel blocker efficacious in animal models of inflammatory and neuropathic pain (*37*), and optimized it for T-type blocking activity based on (i) structural novelty of the class, (ii) demonstrated oral bioavailability and central nervous system penetrance of the backbone, (iii) excellent off-target profile against other ion channels such as the human ERG (hERG) potassium and cardiac sodium $Na_V1.5$ channels, and (iv) relative ease of synthesis. We also sought to improve upon physiochemical properties by enhancing aqueous solubility and lipophilicity.

In vitro potency against the $hCa_V3.2$ T-type channel was achieved by varying regions of the piperazine scaffold designated as M1, M2, and M3 (Fig. 1A). Several small focused libraries were designed, synthesized, and screened with the $hCa_V3.2$ assay, resulting in compounds with IC_{50} (the concentration of a substance required to inhibit the activity of another substance by 50%) values below 500 nM for the $hCa_V3.2$ target. Z121912 is an example of the first generation of this class of T-type channel blocker (Fig. 1B). Many compounds in this piperazine series containing bis(trifluoromethyl)phenyl-acetamide moieties displayed high affinity for the T-type Ca^{2+} channel, although moderate affinity for the hERG potassium channel was also apparent. Further series of piperidine-based analogs were prepared by replacing the benzhydryl moiety with open-chain secondary alcohols (Z2) as well as tertiary amines (Z3). After several iterations of structure-activity relationships based on Z3, three series were identified in the amino methyl piperidine class with the state-dependent fluorescence assay: (i) analogs of Z6 (acidic sulfonamides), (ii) analogs of Z7 (aminoethyl amides), and (iii) analogs of Z941/Z944 (glycinamides). This strategy allowed for the construction of a putative pharmacophore containing a structural moiety that maximized $hCa_V3.2$ inhibition and minimized hERG activity. Testing the new chemical entities in the $hCa_V3.2$ fluorometric imaging plate reader (FLIPR) assay identified Z941 and Z944, and

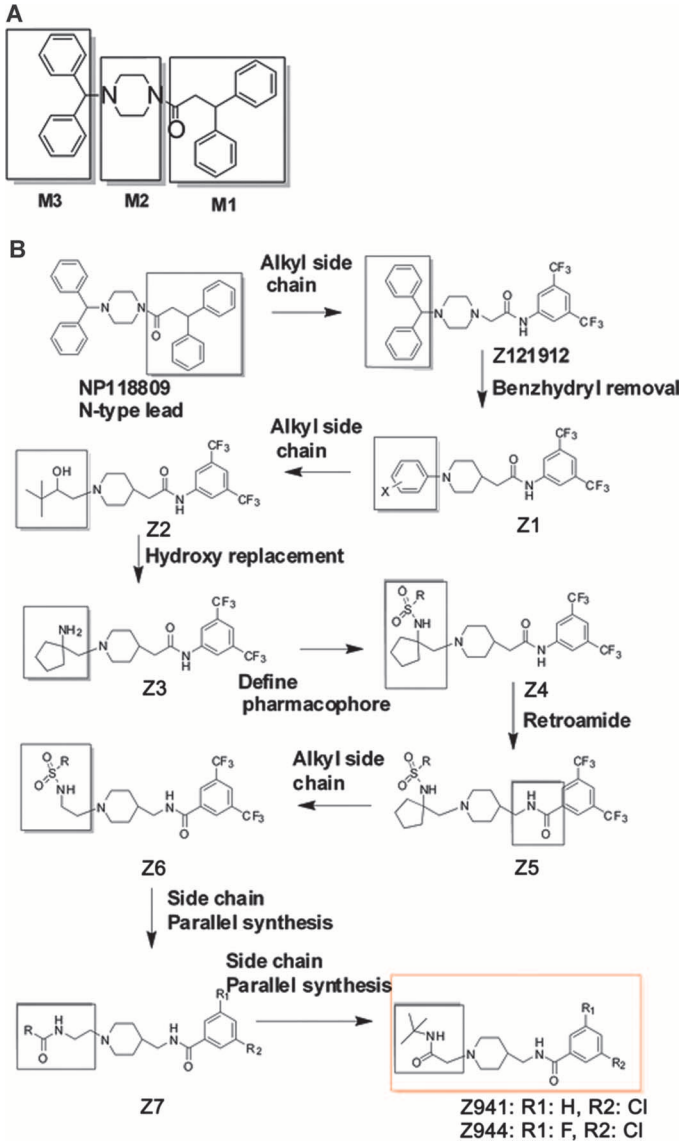

Fig. 1. (**A** and **B**) Summary of the rational design strategy for the identification of Z941 and Z944.

these were compared to ethosuximide and valproate, two first-line anti-absence drugs (*32*). In this assay, both Z941 and Z944 inhibited $hCa_V3.2$ channels with nanomolar affinities (Z941, IC_{50} = 120 nM; Z944, IC_{50} = 50 nM) and exhibited significantly improved potency (~600 to 3800 times higher) compared to ethosuximide (IC_{50} = 70 mM) and valproate (IC_{50} = 190 mM; Fig. 2).

Z944 is highly selective for T-type channel blockade

The selectivity of Z944 was further investigated with a manual patch-clamp assay against the $hCa_V3.1$, $hCa_V3.2$, and $hCa_V3.3$ T-type Ca^{2+} channel isoforms, as well as several other voltage-gated ion channels (see the Supplementary Material). Under conditions producing about 30% channel inactivation, the IC_{50} values for Z944 inhibition of the $hCa_V3.1$, $hCa_V3.2$, and $hCa_V3.3$ T types were all in the submicromolar range (IC_{50} values = 50 to 160 nM; fig. S1). Similar examination of partially inactivated $Ca_V2.2$ channels showed that Z944 was about 70 times more potent for T-type blockade than for blockade of the N-type channel (IC_{50} = 11 μM). Closed-state affinity was also measured, and fits of concentration-dependent response curves yielded IC_{50} values of 130, 540, and 260 nM for the recombinant $hCa_V3.1$, $hCa_V3.2$, and $hCa_V3.3$ channels, respectively (fig. S1). In this regard, the IC_{50} value of Z944 was 2.5- to 4-fold lower for the inactivated state of T-type channels than for the closed state. The blockade of $Ca_V2.2$ channels was also state-dependent (14-fold), with an IC_{50} value of 150 μM for N-type channels in the closed state (fig. S1D).

We also examined the effect of Z944 on the rat $Ca_V1.2$ ($rCa_V1.2$) L type, the hERG potassium channel, and the human $Na_V1.5$ sodium channel ($hNa_V1.5$) to assess its potential to trigger off-target cardiovascular effects (see the Supplementary Material). Z944 showed excellent in vitro selectivity against these targets, exhibiting about 50 to 600 times higher affinity for the neuronal T-type channels than these cardiovascular-related channels ($rCa_V1.2$ IC_{50} = 32 μM; hERG IC_{50} = 7.8 μM; $hNa_V1.5$ IC_{50} = 100 μM; fig. S2).

Z944 was further tested for its potential to affect cardiovascular properties under more physiological conditions. Prolongation of action potential duration (APD) has been associated with ventricular arrhythmia, including torsades de pointes, and therefore, we examined the effects of Z944 on APD on isolated rabbit heart Purkinje fibers (see the Supplementary Material). At a concentration of 0.9 μM (~5- to 18-fold above the IC_{50} values for T-type blockade) (fig. S1), Z944 did not affect APD, action potential amplitude (APA), the maximum rate of depolarization (dV/dt_{max}), or RMP (table S1). At a concentration (9.2 μM) about 58- to 180-fold above the IC_{50} values for inactivated-state T-type blockade, Z944 did not alter RMP, APA, or dV/dt_{max} but shortened the APD (table S1). At the highest concentration tested (27.5 μM; ~170- to 550-fold above the T-type IC_{50} values), Z944 did not alter Purkinje fiber APA or RMP, although it significantly shortened the APD and decreased dV/dt_{max} (table S1).

In another analysis, an in vivo cardiovascular safety pharmacology study was conducted in telemetry-instrumented cynomolgus monkeys receiving, in a Latin four-way crossover design, single oral gavage doses of Z944 (up to 45 mg/kg) (see the Supplementary Material). Z944 was well tolerated at all doses, with no significant changes up to 4 hours after treatment in heart rate, mean arterial pressure, RR intervals, or QTc intervals compared to vehicle-treated animals (table S2). Together, the results of these studies demonstrated that Z944 did not induce prolongation of APD in an in vitro preparation (table S1) and further revealed no adverse effects on quantitative electrocardiogram parameters or arterial pressure in vivo (table S2).

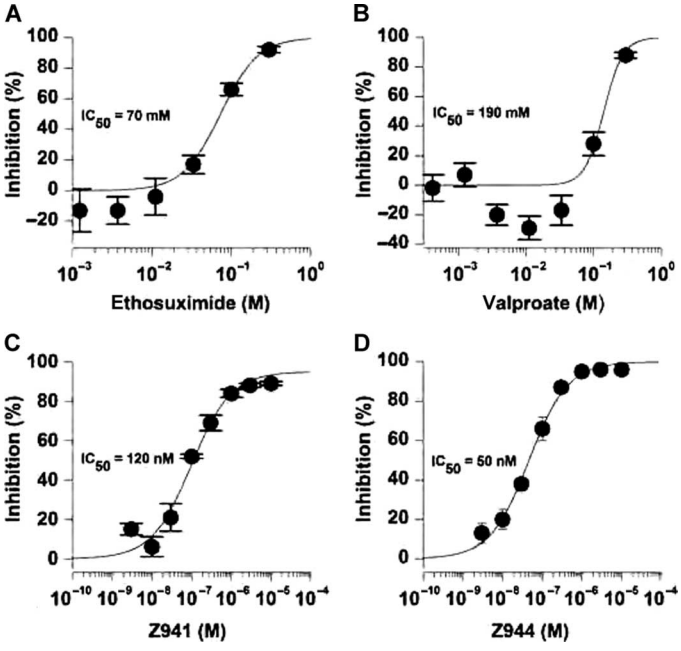

Fig. 2. Concentration-dependent inhibition of $hCa_V3.2$ measured with an inactivated channel state FLIPR assay. (**A**) Ethosuximide IC_{50} inactivated state = 70 mM, slope = 2.1. (**B**) Valproate IC_{50} inactivated state = 190 mM, slope = 4.4. (**C**) Z941 IC_{50} inactivated state = 120 nM, slope = 0.8. (**D**) Z944 IC_{50} inactivated state = 50 nM, slope = 1.5. Data are means ± SD. n = 4 wells per concentration fitted with a logistic function.

Z941 and Z944 potently suppress seizure activity in GAERS

We evaluated Z941 and Z944 in vivo for efficacy against absence seizures in the GAERS model of absence epilepsy (*38*). The anti-absence seizure effects of Z941, Z944, and the two standard-of-care drugs, valproate and ethosuximide, were tested in GAERS by assessing time spent in seizure activity, number of seizures per hour, and average seizure duration. Example EEG traces from GAERS after vehicle, Z944 (10 mg/kg), and ethosuximide (100 mg/kg) treatment are shown in Fig. 3.

After intraperitoneal administration of drugs, significant differences were seen between treatments for the primary endpoint and percent of time spent in seizure activity [$F_{1,7}$ = 13.74; P < 0.0001, one-way repeated-measures analysis of variance (ANOVA); Fig. 4A]. Post hoc analysis showed that compared to vehicle treatment, all test compounds significantly reduced the time spent in seizure (P < 0.05). At both doses tested, Z941 and Z944 significantly reduced the time spent in seizure and, at the highest dose (30 mg/kg), almost completely suppressed seizure expression (85 to 90%). Similar results were observed concerning the number of seizures ($F_{1,7}$ = 13.10; P < 0.0001, one-way repeated-measures ANOVA; Fig. 4B), with both compounds significantly reducing this outcome compared with vehicle (P < 0.05). We also observed significant differences in individual seizure duration at both doses of Z941 and Z944 compared to ethosuximide ($F_{1,7}$ = 5.81; P = 0.0002, one-way repeated-measures ANOVA; Fig. 4C). In contrast, even at 10 to 20 times higher doses than Z941 and Z944, ethosuximide and valproate did not influence seizure duration compared to treatment with vehicle. The effect on seizure duration by Z944 and Z941 was unexpected because previous studies of antiepileptic drugs that suppress seizures in GAERS have all failed to show alterations in seizure duration (*39*–*41*).

This suggested that our T-type channel antagonists may affect SWDs differently than do the standard clinical agents.

Z941 and Z944 have differential effects on the cycle frequency of SWDs compared to ethosuximide

To further investigate the electrophysiological effects of Z941, Z944, and ethosuximide, we assessed their ability to influence the characteristics of SWDs by examining the cycle frequency of SWDs in GAERS during the seizures. A fast Fourier transform (FFT) of Z944 (30 mg/kg), ethosuximide (100 mg/kg), and vehicle during both seizure activity and interictal activity is shown in Fig. 5A. ANOVA analysis revealed significant differences between the treatments in their effects on the cycle frequency of SWDs ($P < 0.0001$; Fig. 5B). Post hoc analysis revealed that both Z941 and Z944 at 30 mg/kg reduced cycle frequency compared with vehicle treatment ($P < 0.001$), an effect that was not observed after ethosuximide treatment at 100 mg/kg ($P > 0.05$). Given that Z941, Z944, and ethosuximide all suppressed seizures, this differential effect, coupled with the differing abilities of these compounds to reduce seizure duration, suggests that Z941 and Z944 blockers act via a different mechanism in the thalamocortical circuitry than does ethosuximide.

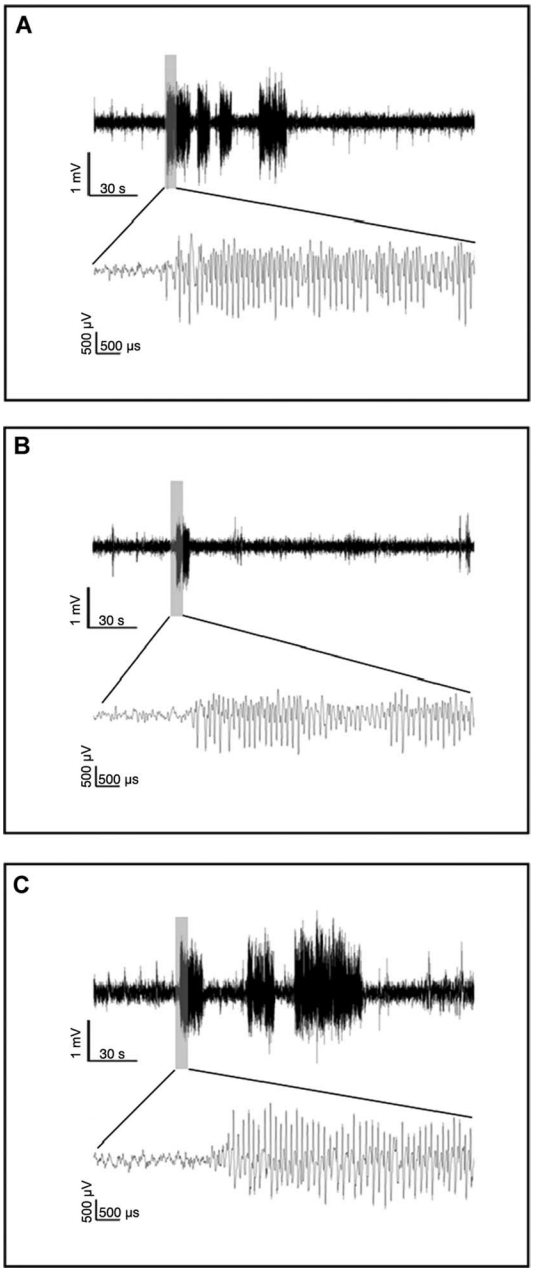

Fig. 3. Effect of Z944 and ethosuximide on EEG. (**A** to **C**) Example EEG traces from GAERS after intraperitoneal treatment with (A) vehicle, (B) Z944 (10 mg/kg), and (C) ethosuximide (100 mg/kg).

Slow (delta) wave activity is not increased by Z944

Delta brainwaves are the largest, slowest waves (<4 Hz) in the EEG and progressively increase during drowsiness and the sleep state. To investigate whether our T-type blockers affected slow wave activity, we quantitated the power of interictal delta wave activity for a 45-min period in freely moving GAERS after drug or vehicle administration. Delta wave activity in GAERS after Z944 (10 mg/kg) ($218.3 \pm 25.8\ \mu V^2$; $n = 8$) or ethosuximide (100 mg/kg) ($216.5 \pm 25.1\ \mu V^2$; $n = 8$) was not significantly different from that in rats after vehicle treatment ($248.7 \pm 22.6\ \mu V^2$; $n = 8$; $P > 0.05$, one-way repeated-measures ANOVA; Fig. 5C). These data indicate that at efficacious doses, Z944 does not suppress seizures in GAERS by increasing delta wave activity or inducing drowsiness.

Z941 and Z944 are well tolerated with minimal neurotoxic effects in GAERS

Behavior was assessed in GAERS animals every 15 min to detect any adverse effects of Z941 and Z944 (measurements were made for 60 min before and 120 min after drug administration). A score of 0 indicated normal movement, and a score of 4 indicated major motor abnormalities. The eight scores (one experiment per rat) were averaged,

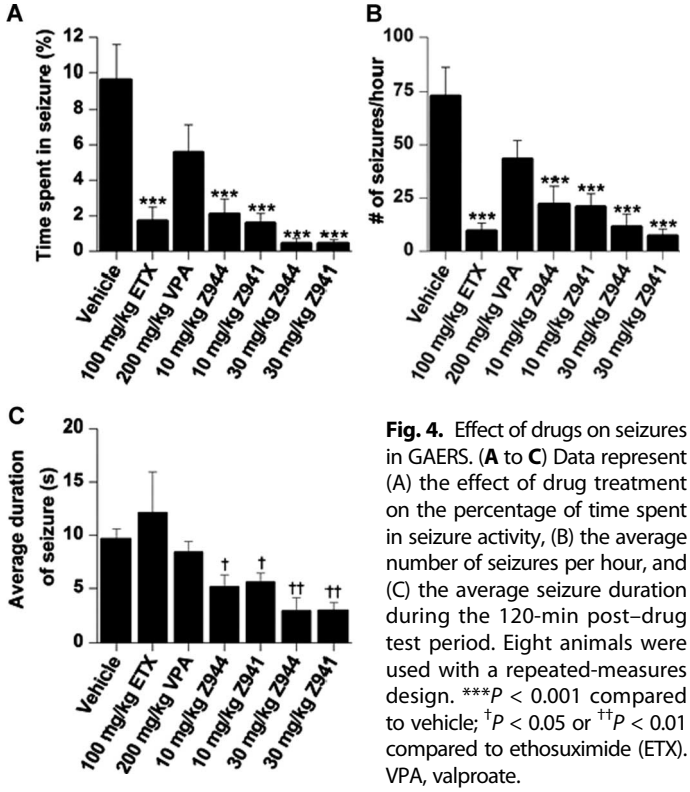

Fig. 4. Effect of drugs on seizures in GAERS. (**A** to **C**) Data represent (A) the effect of drug treatment on the percentage of time spent in seizure activity, (B) the average number of seizures per hour, and (C) the average seizure duration during the 120-min post–drug test period. Eight animals were used with a repeated-measures design. ***$P < 0.001$ compared to vehicle; †$P < 0.05$ or ††$P < 0.01$ compared to ethosuximide (ETX). VPA, valproate.

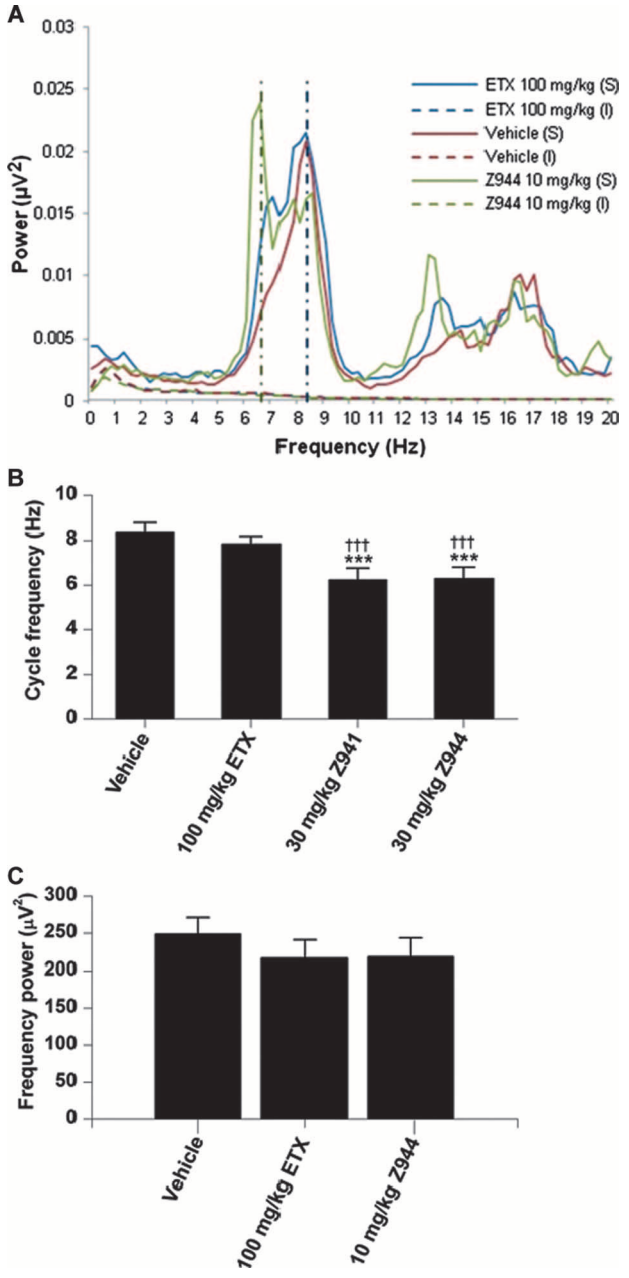

Fig. 5. Effect of drugs on cycle frequency of SWDs. (**A**) FFT of Z944, ethosuximide (ETX), and vehicle during both seizure (S) activity and interictal (I) activity. The graph shows a shift in peak cycle frequency power from 8 to 6.5 Hz during seizure activity in Z944 (30 mg/kg)–treated animals when compared to ethosuximide (100 mg/kg) and vehicle. FFTs were averaged over five interictal or seizure periods for each treatment. (**B**) Mean cycle frequency of the SWDs (cycles per second) for the highest dose of the two Ca^{2+} channel blockers Z941 (30 mg/kg) and Z944 (30 mg/kg) compared to ethosuximide (100 mg/kg) and the vehicle. The cycle frequency of SWDs was obtained by measuring the average cycle frequency of the first 10 clean seizures during the 120-min target period. (**C**) Quantification of the power of delta frequency activity (0 to 3.75 Hz) on the EEG recordings during interictal periods in GAERS acquired for a 45-min period after intraperitoneal administration of Z944 (10 mg/kg), ethosuximide (100 mg/kg), or vehicle while the animals were awake and freely moving. The frequency power is plotted as mean ± SEM, $n = 8$ animals. ***$P < 0.001$ compared to vehicle; $^{\dagger\dagger\dagger}P < 0.001$ compared to ethosuximide.

and then group means were calculated for each dose. All treatments were well tolerated by the animals, and the maximum toxicity score recorded after any of the treatments was 1 over the 4-week crossover period of treatment. The median sedation score on the five-point scale (with 0 being no sedation and 4 being major sedation) for Z944 was 0.19 (10 mg/kg) and 0.14 (30 mg/kg) and for Z941 was 0.08 (10 mg/kg) and 0.13 (30 mg/kg). These were not significantly different from the median score for valproate (0.25), ethosuximide (0.19), or vehicle (0.05) treatments ($P = 0.060$, Friedman ANOVA). Animal weight and also behavior when handled were monitored for the duration of the experimental period. Additionally, animals were assessed by observation for any adverse effects of drugs on grooming, fur appearance, gait, and excretion. No significant long-term adverse effects were observed for any of these parameters over the 4-week experimental period during which drugs were administered.

Z944 T-type Ca^{2+} channel blocker inhibits burst firing in nRT neurons

In GAERS, CaV3.2 mRNA and T-type Ca^{2+} currents are both elevated in nRT neurons (*12*, *42*), and associate with an underlying missense mutation (R1584P) in the $Ca_V3.2$ channel; thus, we examined the effects on Z944 in both nRT neurons and the cloned $rCa_V3.2$ containing the R1584P mutation. Specifically, the R1584P GAERS mutation induces a splice variant–specific enhanced rate of recovery from inactivation in $Ca_V3.2$ channels containing exon 25 (*21*). Application of 1 μM Z941 or 0.4 μM Z944 did not significantly alter the rate of recovery of $rCa_V3.2$ (+25, R1584P) mutant channels from inactivation (Fig. 6). However, the fractional recovery from inactivation was significantly ($P < 0.05$) reduced at recovery interpulse intervals greater than 1280 ms for Z941 and 2560 ms for Z944 compared to control currents recorded in 0.02% dimethyl sulfoxide (DMSO) (solvent used to prepare compounds), which were slightly facilitated (P2/P1 current = 1.10). On average, recovery was 89% for Z941 and 93% for Z944 at a 5120-ms interpulse interval compared to the DMSO control. Z944, in particular, was further examined for possible effects on fast inactivation (fig. S3) and on the kinetics of activation and deactivation (table S3). With the exception of a slight alteration in the slope of the fast inactivation curve, no significant effects were observed on these parameters. Given the observed state-dependent effects by Z944 on the T-type channels (fig. S1), we further tested whether $hCa_V3.2$ inhibition varied with the frequency of stimulation. Three 5-s trains of action potentials at a frequency of either 1 or 20 Hz were applied to cells expressing $hCa_V3.2$ during perfusion of control solution and solution containing 100 nM Z944. The degree of block was measured by comparing the peak amplitude of a test pulse applied immediately after the trains of action potentials under control conditions with the peak amplitude of a similar test pulse applied during perfusion of 100 nM Z944 (fig. S4). Z944 inhibited a significantly greater percentage of $hCa_V3.2$ channels during 20-Hz stimulation than during 1-Hz stimulation (42 and 33% inhibition, respectively; $P < 0.05$; table S4).

Neurons of the nRT normally express a combination of $Ca_V3.2/Ca_V3.3$ currents, and in both humans and GAERS, T-type channels in nRT neurons are thought to be critically involved in absence seizures by generating depolarizing bursts that in turn hyperpolarize thalamocortical neurons and thereby cause recovery of inactivated T-type Ca^{2+} channels, leading to increased membrane excitability (*43*–*46*). This excitability can then lead to increased burst firing in thalamocortical neurons and

the propagation of SWDs in the thalamocortical system (*10*). In this regard, we examined the ensemble $Ca_V3.2/Ca_V3.3$ T-type Ca^{2+} currents (Fig. 7) and burst-firing properties (Fig. 8) of nRT neurons for sensitivity to Z944 in thalamic slice preparations from both GAERS and NEC animals (Tables 1 and 2). Under voltage-clamp conditions, Z944 potently and completely inhibited the isolated T-type Ca^{2+} currents, induced by a −90- to −50-mV voltage step, in both NEC and GAERS animals (IC_{50} values of 122 and 110 nM, respectively; Fig. 7A). Current density analysis revealed that T-type Ca^{2+} currents were blocked in both NEC and GAERS (Fig. 7B) in a similar manner by Z944 (10 μM). The small residual current present between −30 and 0 mV after Z944 application (Fig. 7B) is likely a result of a low level of contamination from HVA currents at these more depolarized test potentials. The inhibition by Z944 was largely nonreversible in nRT neurons of both strains after 30-min washout (Fig. 7C).

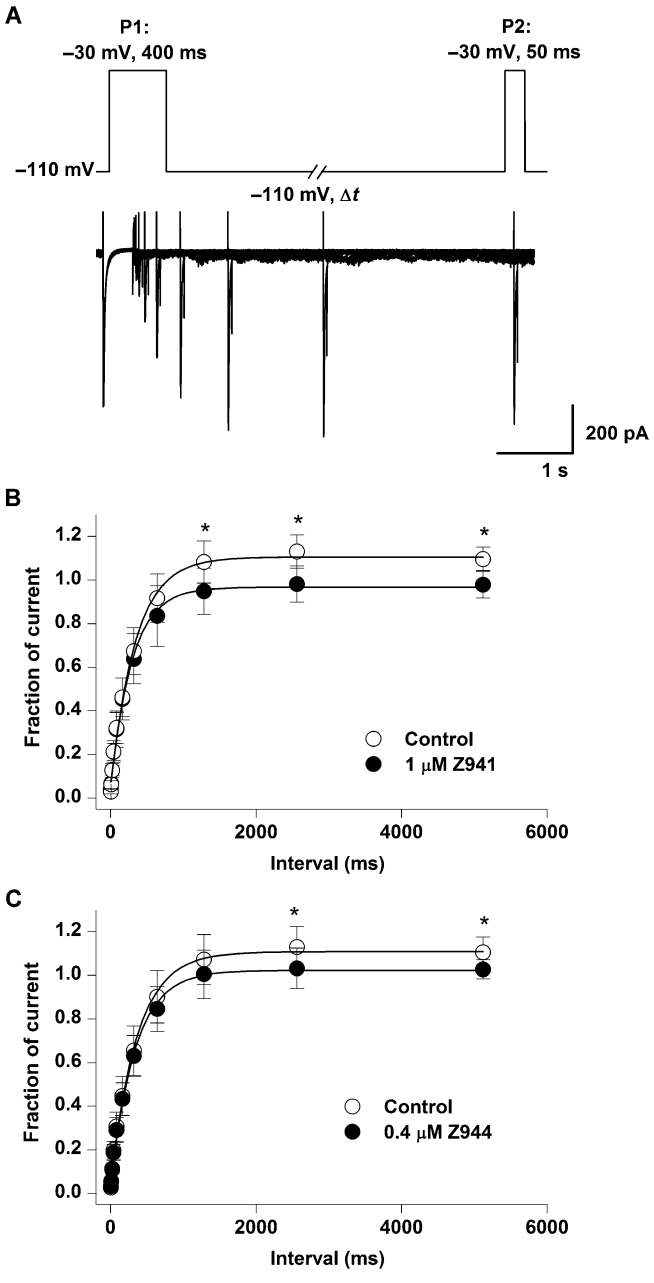

Fig. 6. Effect of Z941 and Z944 on $rCa_V3.2$. (**A**) The kinetics of recovery from inactivation were determined with a two-pulse protocol (P1, 400 ms to −30 mV; P2, 50 ms to −30 mV) with a variable interpulse interval (5 to 5120 ms) applied every 20 s from a holding potential of −110 mV. Below are representative $Ca_V3.2$ channel current traces. (**B** and **C**) The time course of recovery from channel inactivation was fitted with a single exponent for currents recorded in the presence or absence of Z941 and Z944. t = 354 ± 80 ms recorded in 0.02% DMSO, 312 ± 71 ms in 1 μM Z941 (B), and 354 ± 80 ms in 0.4 μM Z944 (C). Data are means ± SD. n = 5 to 11 cells per concentration. *P < 0.05, Student's t test, compared to 0.02% DMSO control.

T-type Ca^{2+} currents underlie the low-threshold spike that induces burst firing in neurons. Thus, we assessed the effects of Z944 on the burst-firing properties of GAERS and NEC nRT neurons. Burst firing was induced by applying depolarizing steps of increasing magnitude (10-pA increments) until burst or tonic action potential firing was elicited. Z944 was applied at 1 μM, which blocks ~95% of the T-type Ca^{2+} channel current for up to 20 min. Z944 completely abolished burst firing in GAERS nRT neurons without inhibiting their ability to fire action potentials upon injection of an increased magnitude depolarizing current (Table 1 and Fig. 8, A and B). The charge required to induce action potential firing (calculated by current injected × time to first action potential) was significantly increased by Z944, and the burst inflection point (where the neuron depolarizes exponentially immediately before firing an action potential) was significantly depolarized compared to before application and to DMSO controls in both strains, consistent with a loss of LVA current. Furthermore, the number of action potentials fired during the burst time scale of 500 ms was significantly reduced, without alteration in the mean action potential maximum membrane potential (Table 1). In addition, Z944 had no effect on the RMP or input resistance, confirming that the effects were not due to modulation of passive neuronal properties. The overall effect of Z944 was to effectively prevent nRT neurons from burst firing without affecting their ability to fire tonically, although Z944 did increase the threshold level of the injected charge required for firing. To confirm that the observed reduction in excitability was due to a direct effect of Z944 on T-type Ca^{2+} currents and therefore the low-threshold spike, we examined neuronal activity in the presence of 600 nM tetrodotoxin (TTX) to block sodium currents and therefore action potentials. In the presence of 1 μM Z944, we could not elicit a low-threshold spike generated by T-type Ca^{2+} channels even when injecting a stimulating current that was double the amperage of those used to elicit a low-threshold spike in the absence of Z944 (Table 2 and Fig. 8C, inset).

DISCUSSION

To identify high-affinity T-type Ca^{2+} channel blockers, we developed a $Ca_V3.2$ T-type channel fluorescence-based assay that used the Ca^{2+}-sensitive dye Fluo-4 and, when combined with a coexpressed $K_{ir}2.3$ inward rectifier, reliably differentiated between test compounds on the basis of their affinity for distinct channel states. The channel state was controlled by varying the extracellular potassium concentration to modulate the cell membrane potential to alter the channel occupancy state. At a low external potassium concentration, the HEK cell membrane potential is hyperpolarized, and T-type Ca^{2+} channels preferentially reside in the closed-channel conformation. Progressive increases in extracellular potassium result in a greater degree of T-type Ca^{2+} chan-

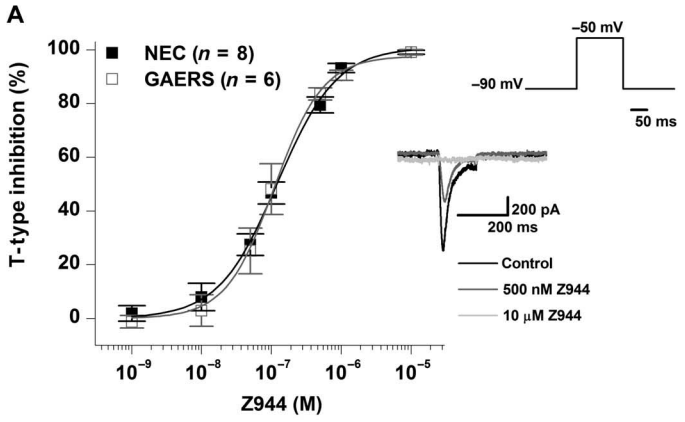

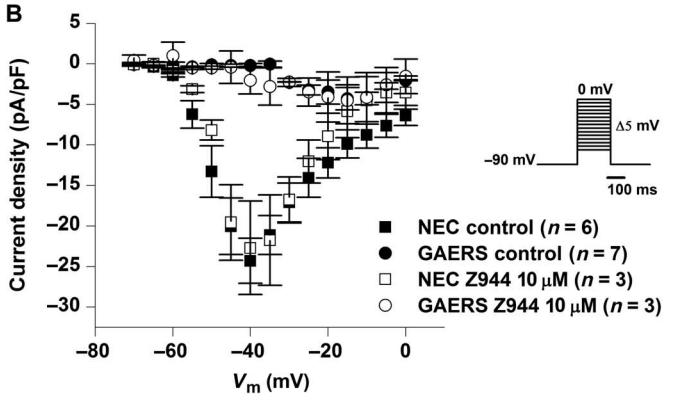

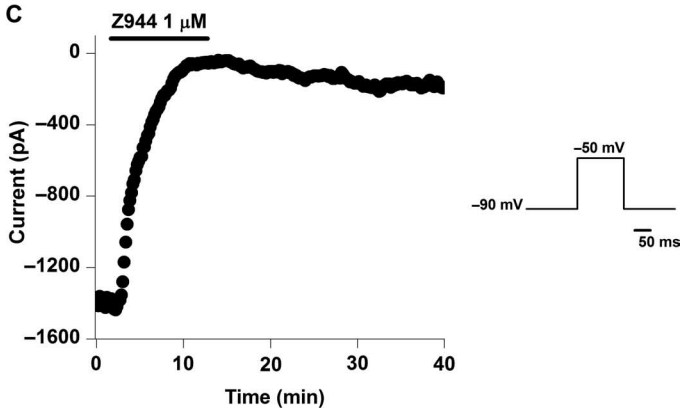

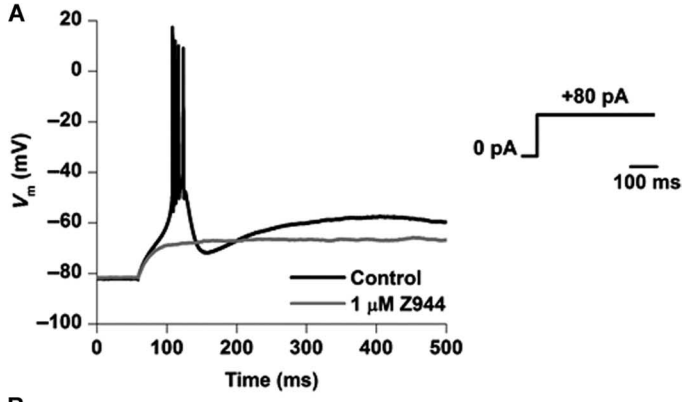

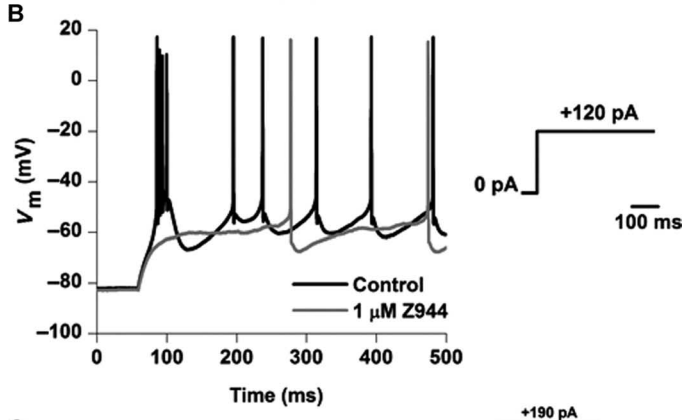

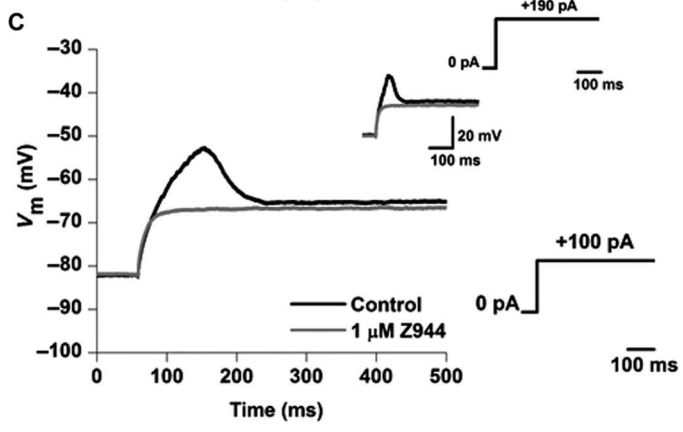

Fig. 7. Effect of Z944 on thalamic nRT T-type Ca^{2+} currents. (**A**) Concentration-dependent response curve generated by inhibition of the mixed $Ca_V3.2/Ca_V3.3$ current expressed in NEC (filled squares; $n = 8$) and GAERS (empty squares; $n = 6$) nRT neurons by Z944. Inset: Representative traces of a GAERS nRT T-type Ca^{2+} channel currents in the absence (black trace) or presence of 500 nM Z944 (dark gray trace) and 10 μM Z944 (light gray trace). Currents were elicited by a step to −50 mV from a holding of −90 mV for a duration of 150 ms every 10 s until a stable baseline was achieved, then various concentrations of Z944 were applied. (**B**) Current density plot demonstrating GAERS nRT currents in the absence (filled circles; $n = 7$) and presence (open circles; $n = 3$) of 10 μM Z944. Inset: Currents were elicited at various potentials beginning at −70 mV (duration, 200 ms) and then in increasing increments of 5 mV from a holding potential of −90 mV every 10 s. (**C**) Representative time course demonstrating nonreversible inhibition of GAERS nRT T-type Ca^{2+} channel currents under voltage clamp in response to 1 μM Z944 and wash off. Inset: Currents were elicited by a step to −50 mV from a holding of −90 mV for a duration of 150 ms every 10 s. Data are means ± SEM.

Fig. 8. Effect of Z944 on burst firing in thalamic nRT neurons. (**A**) Representative traces from a GAERS nRT neuron in current clamp, showing voltage responses to a depolarizing current (+80 pA; inset), which is the threshold for burst firing in control (black trace) but the subthreshold for firing after application of 1 μM Z944 (gray trace). (**B**) Representative traces from the same GAERS nRT neuron as in (A), showing voltage responses to a depolarizing current of greater magnitude (+120 pA; inset), which is suprathreshold for burst firing in control (black trace) but threshold for tonic firing after application of 1 μM Z944 (gray trace). (**C**) Representative traces from a GAERS nRT neuron in the presence of 600 nM TTX, showing voltage responses to a depolarizing current (+100 pA; lower inset), which is threshold for low-threshold spiking in control (black trace) but subthreshold for low-threshold spiking after application of 1 μM Z944 (gray trace). Upper inset: Representative traces from the same GAERS nRT neuron, showing voltage responses to a depolarizing current of greater magnitude (+190 pA; inset), which is suprathreshold for low-threshold spiking in control (black trace) and still subthreshold after application of 1 μM Z944 (gray trace).

Table 1. Burst properties of thalamic nRT neurons. R_{in}, input resistance.

	NEC			GAERS		
	Control (n = 5)	**Z944 (1 μM) (n = 5)**	**DMSO (1:10,000) (n = 3)**	**Control (n = 5)**	**Z944 (1 μM) (n = 5)**	**DMSO (1:10,000) (n = 3)**
Threshold current for firing (pA)	70.0 ± 14.8	154 ± 23.4*	80.0 ± 15.3	86 ± 12.1	150 ± 19.5†	102.5 ± 7.5
Time to first action potential (ms)	118.9 ± 3.5	114.8 ± 27.4	85.9 ± 24.4	99.5 ± 12.3	157.2 ± 54.2	100.0 ± 12.7
Charge to first action potential (nC)	8.4 ± 1.8	15.4 ± 1.3*	7.2 ± 2.9‡	8.2 ± 1.1	19.7 ± 2.7*	10.14 ± 1.2‡
Burst inflection point (mV)	−66.0 ± 1.9	−52.3 ± 3.5†	−62.9 ± 1.7‡	−64.5 ± 1.8	−52.7 ± 3.1†	−64.9 ± 4.6‡
Threshold number action potentials	4.8 ± 0.8	1.0 ± 0.0§	5.3 ± 1.9‡	4.4 ± 0.7	1.2 ± 0.2†	5.3 ± 1.5‡
Mean action potential peak V_m (mV)	9.1 ± 4.0	12.6 ± 2.8	3.7 ± 10.3	8.7 ± 3.7	8.3 ± 5.8	1.2 ± 3.7
RMP (mV)	−82.1 ± 2.0	−82.4 ± 2.1	−81.2 ± 1.0	−79.9 ± 2.4	−80.1 ± 2.3	−81.4 ± 4.2
R_{in} (megohm)	188.2 ± 28.8	163.0 ± 14.11	183.8 ± 36.5	148.7 ± 12.7	162.3 ± 18.3	161.8 ± 22.3

*P < 0.05, paired t test, control versus 1 μM Z944. †P < 0.005, paired t test, control versus 1 μM Z944. ‡P < 0.05, unpaired t test, 1 μM Z944 versus DMSO. §P < 0.001, paired t test, control versus 1 μM Z944.

Table 2. Low-threshold spike (LTS) properties of nRT neurons.

	NEC		GAERS	
	Control (n = 5)	**Z944 (1 μM) (n = 5)**	**Control (n = 5)**	**Z944 (1 μM) (n = 5)**
LTS magnitude (mV)	19.5 ± 5.2	0.4 ± 0.6*	19.3 ± 4.3	−0.4 ± 0.4*
RMP (mV)	−78.2 ± 1.9	−76.7 ± 1.7	−76.9 ± 2.7	−76.2 ± 3.7
R_{in} (megohm)	183.2 ± 31.5	175.7 ± 39.6	183.5 ± 25.4	153.2 ± 21.1

*P < 0.005 (paired t test).

nel inactivation. In epilepsy, and in particular absence epilepsy, T-type Ca^{2+} channels are critical for the generation of burst firing in thalamic neurons, which leads to generalized SWDs in cortical and thalamic structures (*46*–*48*). We predicted that this anomalous increase in neuronal activity (burst firing), which drives channels into the inactivated state, would be inhibited by agents that target the inactivated channel state. Such agents are predicted to reduce the activity of neurons undergoing high-frequency firing while largely sparing low-frequency firing neurons in which channels would be predominantly in the closed-channel state.

Deriving knowledge from a previous pharmacophore that blocked the N-type Ca^{2+} channel (*37*) and combining this with a high-throughput fluorometric assay, we identified two high-affinity submicromolar blockers, Z941 and Z944, which had preferential affinity for T-type Ca^{2+} channels in their inactivated state. Z944 also inhibited $Ca_V3.2$ channels in a frequency-dependent manner, as well as completely suppressed burst firing of thalamic reticular nucleus neurons.

In the well-established GAERS absence epilepsy model, the two small-molecule, organic T-type blockers Z941 and Z944 reduced seizure activity and had pronounced effects on the electrophysiological characteristics of SWDs. Further, in thalamic slices, Z944 eliminated the burst firing in nRT neurons by abolishing low-threshold spiking. It is likely that the excitability of other neural substrates that contribute to SWDs such as neocortical and thalamocortical neurons, which also exhibit burst firing evoked by low-threshold Ca^{2+} potentials (*43*, *48*–*53*), is similarly affected by our T-type Ca^{2+} channel blockers. The marked effect of Z941 and Z944 on seizures in GAERS may in part be a result of their submicromolar affinity for all three T-type channel isoforms; they are about 600 to 3800 times more potent than that for ethosuximide and valproate. Direct infusion of ethosuximide into the perioral region, but not into the thalamus, of GAERS immediately reduces SWDs (*54*–*56*). Ethosuximide similarly inhibits all three T-type Ca^{2+} channel subtypes (*15*), and its observed effects in vivo may at least in part result from inhibition of T-type currents in the neocortex, a region in which the $Ca_V3.1$ and $Ca_V3.3$ isoforms are diffusely expressed in most layers, and $Ca_V3.2$ expression is restricted to layer 5 cortical pyramidal neurons. Local oscillations originating in perioral somatosensory neurons of layer 5/6 have been proposed to lead to the generation of SWDs, which then propagate to other cortical and thalamic nuclei (*57*–*61*).

Inhibition of the $Ca_V3.1$ T-type channel also likely contributes to the anti-absence effect of Z941 and Z944; $Ca_V3.1$ channels have been implicated in the generation of absence seizures and epilepsy by the finding that $Ca_V3.1$ knockout mice are resistant to baclofen-induced SWDs (*17*). Additionally, mice that result from cross-breeding $Ca_V3.1$ knockout mice with other mutant mice that exhibit absence seizures show strong or complete suppression of cortical SWD paroxysmal activity (*18*). Conversely, overexpression of $Ca_V3.1$ channels in mice promotes frequent bilateral cortical SWDs and causes elevated T-type Ca^{2+} currents in thalamocortical neurons (*19*). Given the potency of Z941 and Z944 at the three T-type isoforms, it is probable that these compounds suppress burst firing not only in the nRT but also in the thalamocortical neurons of the sensory thalamus. For example, neurons of the ventrobasal thalamus project to and receive projections from the somatosensory cortex and are also intrinsically involved in absence seizure propagation. Because these neurons predominantly express the $Ca_V3.1$ isoform, Z941 and Z944 may have anti-absence seizure effects on this region in addition to those observed in the nRT.

In further support of the notion that pan–T-type channel blockade is relevant to control of absence seizures, the $Ca_V3.2$ T-type isoform has also been implicated in the pathogenesis of absence epilepsy; $Ca_V3.2$ mRNA expression (*42*) and T-type currents (*12*) are both elevated in

the nRT neurons of the GAERS model of absence epilepsy (*10*, *20*). Additionally, in a study of WAG/Rij rats, which also display cortical EEG patterns characteristic of absence epilepsy (*62*), a mixed $Ca_V3.1$ and $Ca_V3.3$ blocker dose-dependently reduced the total time spent in seizures. Elevated T-type currents have also been reported in murine models of spontaneous absence epilepsy, in which crossbreeding with $Ca_V3.1$ knockout mice results in animals with marked or complete suppression of cortical SWD paroxysmal activity (*18*, *63*, *64*). Overall, Z941 and Z944 likely target the predominant neural circuitry involved in SWDs by inhibiting the ictogenic properties of the cortical neurons, as well as by disrupting the resonant circuitry of the thalamocortical and nRT neurons, all of which differentially express multiple T-type channel isoforms.

Unlike ethosuximide, Z941 and Z944 reduce both the duration and the cycle frequency of the SWDs in GAERS, suggesting that ethosuximide may exert its anti-absence effect through a different mechanism. Although ethosuximide is thought to exert its anti-absence actions through T-type channel blockade, this notion has been questioned by recent work demonstrating its actions on other voltage-gated channels implicated in epilepsy pathophysiology (*16*). Indeed, ethosuximide inhibits persistent voltage-gated Na^+- and Ca^{2+}-activated K^+ currents in thalamic and cortical pyramidal neurons in layer V (*14*, *16*). Ethosuximide treatment has also been reported to result in an increase in γ-aminobutyric acid (GABA) levels and a decrease in glutamate levels in the motor cortex in a genetic rat model of absence epilepsy (*65*). One potential explanation for the differential effect on the cycle frequency of Z944 compared with ethosuximide is Z944's ability to reduce recovery from channel inactivation, possibly by stabilizing channels in the inactivated state. During SWDs, T-type Ca^{2+} channels are likely driven repeatedly into the inactivated state, which in the presence of compounds such as Z941 and Z944 would be stabilized, thereby reducing the availability of channels and slowing the cycle frequency. Although the clinical significance of the reduction in cycle frequency remains to be determined, it appears that Z941 and Z944 affect SWDs in a different manner than does ethosuximide.

Low-threshold currents driven by T-type Ca^{2+} channels in the thalamocortical neurons are believed to play a role in sleep (*52*). Mice in which the $Ca_V3.1$ gene has been deleted show impaired spindle and delta waves that are generated and propagated by thalamic neurons during nonrapid eye movement sleep, although slow waves originating from the cortex are unaffected (*66*). In addition, deletion of $Ca_V3.1$ in the thalamus of mice results in destabilization of sleep, with animals experiencing frequent arousals (*67*). Conversely, a compound identified as a pan–T-type Ca^{2+} channel blocker (TTA-A2) reduces wakefulness and is proposed to enhance sleep in mice (*68*). At seizure-suppressing doses, we noted no significant sedative effects in Z941- or Z944-treated GAERS. Consistent with this, Z944 did not increase delta wave activity on cortical EEG recordings in freely moving GAERS. Thus, it appears that structurally distinct classes of T-type antagonists can affect sleep architecture in different manners, with the piperidine glycinamides that we report here selectively reducing absence seizure activity without enhancing sleep activity.

Epileptic seizures exhibit different properties and involve multiple distinct brain regions. Mechanistically, we have thus far examined Z944 action only as it relates to nRT T-type currents and excitability, and its effects on other pathophysiological relevant cell types in the ventrobasal thalamus and somatosensory cortex have yet to be assessed. A large percentage of absence patients are pharmacoresistant to first-line human agents such as ethosuximide and valproate. At this point, we cannot predict whether Z944, as a high-affinity, pan–T-type blocking compound that also exhibits state- and frequency-dependent effects, will be an alternative treatment for pharmacoresistant patients. Further, whether the pronounced effects of Z944 toward absence seizures in the highly inbred GAERS model translate to the more complex underlying genetics and pathophysiology of human seizures will need to be assessed in patients.

On the basis of its overall favorable preclinical on- and off-target activities both in vitro and in animal models, Z944 has been selected for progression into phase 1 human studies to assess safety and exposure. Although it is a promising clinical candidate, there remain a number of unknowns concerning the development of Z944 as a therapeutic for absence epilepsy. These include obtaining adequate exposure levels in human plasma and brain as well as assessment of short- and long-term adverse effects after repeated oral administration. T-type Ca^{2+} channels may play a role in seizure phenotypes other than absence seizures (for example, partial seizures) (*69*, *70*), and these, as well as other diseases with T-type channel involvement such as pain (*71*), may also benefit from this approach.

Together, our results substantiate the pivotal role of T-type Ca^{2+} channels in the generation and maintenance of SWDs in absence seizures. Our automated, high-throughput assay and rational backbone-based drug design strategy resulted in the identification of high-affinity T-type channel blockers that both effectively attenuate thalamic burst firing and are highly efficacious in the GAERS model of absence seizures.

MATERIALS AND METHODS

Generation of stable cell line expressing recombinant voltage-gated ion channels

See the Supplementary Materials.

High-throughput $hCa_V3.2/K_{ir}2.3$ T-type fluorescence assay

Cells were plated in 384-well, clear-bottom, black-walled, poly-D-lysine–coated plates (Becton-Dickinson) 2 days before use in the FLIPR assay. Cells (100 μl) (1.2×10^6 cells/ml) containing doxycycline (Sigma-Aldrich, 1.5 μg/ml, to induce channel expression) were added to each well with a Multidrop (Thermo Scientific) and were maintained in a 5% CO_2 incubator at 37°C. On the morning of the assay, cells were transferred to a 5% CO_2 incubator at 29°C.

Cells were washed with a wash buffer containing 118 mM NaCl, 18.4 mM Hepes, 11.7 mM D-glucose, 2 mM $CaCl_2$, 0.5 mM $MgSO_4$, 4.7 mM KCl, and 1.2 mM KH_2PO_4 (pH adjusted to 7.2 with NaOH). The fluorescent indicator dye Fluo-4 (4.4 μM) (Invitrogen), prepared in pluronic acid (Sigma-Aldrich), was loaded into the wells and incubated for 45 min at 29°C in 5% CO_2. Cells were then rinsed with a 7.6 mM KCl inactivated-state buffer (130.9 mM NaCl, 10 mM Hepes, 10 mM D-glucose, 1 mM $CaCl_2$, and 7.6 mM KCl, pH adjusted to 7.4 with NaOH). Concentration-dependent response curves were generated from 5 mM stock solutions prepared in DMSO (Sigma-Aldrich) and diluted in the 7.6 mM KCl buffer and incubated for 20 min at 29°C in 5% CO_2. Calcium entry was evoked with the addition of 14.5 mM KCl stimulation buffer (126 mM NaCl, 10 mM Hepes, 10 mM D-glucose, 1 mM $CaCl_2$, and 14.5 mM KCl, pH 7.4 adjusted with NaOH). A change in the Fluo-4 fluorescence signal was assessed with a FLIPR instrument (Molecular Devices) for 3 min after the elevation of

extracellular KCl using an illumination wavelength of 470 to 495 nm with emissions recorded at 515 to 575 nm.

Concentration-dependent response curves were obtained by comparing the fluorescence signal in the presence of compound and fitted with a logistic function (Eq. 1) to obtain the IC_{50} value of the relative light unit (RLU) signal with OriginPro v.7.5 software (OriginLab).

$$y = \frac{L^n}{K_d + L^n} \quad (1)$$

To assess the quality of the FLIPR assays, we used the *Z* factor (Eq. 2) to quantify the suitability of the assay conditions using the following equation:

$$Z = 1 - \frac{3\ SD_{sample} + 3\ SD_{control}}{mean_{sample} - mean_{control}} \quad (2)$$

Data are expressed as means ± SD.

$Ca_V3.2$ T-type channel voltage-clamp recordings

Before $hCa_V3.2$ T-type Ca^{2+} currents were recorded, the culture medium in 35-mm dishes was replaced with extracellular solution containing 142 mM CsCl, 10 mM D-glucose, 2 mM $CaCl_2$, 1 mM $MgCl_2$, and 10 mM Hepes (pH adjusted to 7.4 with CsOH). Borosilicate glass patch pipettes pulled (2 to 6 megohms) from borosilicate glass with a P-97 puller (Sutter Instruments) and fire-polished (Narishige) were backfilled with intracellular containing 126.5 mM Cs-methanesulfonate, 2 mM $MgCl_2$, 10 mM Hepes, 11 mM EGTA, and 2 mM Na-ATP (adenosine triphosphate) (pH adjusted to 7.3 with CsOH), and experiments were performed in the whole-cell configuration with an Axopatch 200B patch-clamp amplifier (Molecular Devices) at room temperature (~21°C). pCLAMP 9 or 10 (Molecular Devices) was used to create, record, and subtract leak and uncompensated capacitance currents online with a P/4 protocol. Recordings were low pass–filtered at 1 kHz (−3-dB four-pole Bessel filter) and digitized with a Digidata 1320A, 1322A, or 1440A (Molecular Devices) at 20 kHz. Test compounds were prepared as 10 mM stock solutions in DMSO and diluted in extracellular buffer. Solutions were applied by a gravity-driven multibarreled array of custom microfils (World Precision Instruments) connected by Teflon tubing (24 gauge, Scientific Commodities) to Teflon syringes (Savillex) and controlled by solenoid valves (VC-8 valve controller, Warner Instruments). Details of the voltage protocols are provided in the Results section and the Supplementary Material. Data were analyzed and fitted with OriginPro v.7.5 software (OriginLab). $Ca_V3.2$ T-type Ca^{2+} channel currents were fitted with the applicable equations: logistic fit to obtain IC_{50} values (Eq. 3) or Boltzmann function for determining the voltage dependence of channel activation and inactivation (Eq. 4).

$$y = \left[\frac{max - min}{1 + \left(\frac{[drug]}{IC_{50}}\right)^{n_H}}\right] + min \quad (3)$$

$$y = \left(\frac{max - min}{1 + e^{(V_m - V_h)/k}}\right) + min \quad (4)$$

Data are expressed as means ± SD.

Thalamic slice patch-clamp recordings

P10-P20 GAERS and NEC rats (male and female; bred by the Zoology Department at The University of British Columbia, Canada) were briefly anesthetized with halothane and killed by cervical dislocation, and the brains were rapidly removed. Brain tissue was glued to a cutting chamber, which was filled with ice-cold sucrose solution containing 234 mM sucrose, 24 mM $NaHCO_3$, 1.25 mM NaH_2PO_4, 11 mM glucose, 2.5 mM KCl, 0.5 mM $CaCl_2$, and 10 mM $MgSO_4$, bubbled with 95% O_2/5% CO_2. Horizontal brain slices (350-μm thick) were cut from the level of the ventral nRT and incubated for a minimum of 1 hour at 34°C in recording solution containing 126 mM NaCl, 2.5 mM KCl, 26 mM $NaHCO_3$, 1.25 mM NaH_2PO_4, 2 mM $CaCl_2$, 2 mM $MgCl_2$, 10 mM glucose, 1 mM kynurenic acid, and 0.1 mM picrotoxin, bubbled with 95% O_2/5% CO_2. Slices were then transferred to the recording chamber superfused with recording solution and maintained at 33°C to 35°C. nRT neurons were visualized with a DIC microscope (Axioskop 2-FS Plus, Carl Zeiss) and infrared camera (IR-1000, Dage-MTI) and visually identified by their morphology and orientation.

All recordings were undertaken with a Multiclamp 700B amplifier and pCLAMP software version 9 (Molecular Devices). The recording chamber was grounded with an Ag/AgCl pellet. Whole-cell voltage-clamp recordings were undertaken with fire-polished borosilicate glass pipettes (3 to 5 megohms) filled with an intracellular of composition containing 140 mM Cs-methanesulfonate, 10 mM Hepes, 0.5 mM $MgCl_2$, 11 mM EGTA, 1 mM $CaCl_2$, 5 mM tetraethylammonium-Cl, 4 mM MgATP, and 0.5 mM NaGTP (sodium guanosine triphosphate) (pH adjusted to 7.2 with CsOH and osmolarity adjusted to 290 mOsm/kg with D-mannitol). TTX (600 nM), 4-aminopyridine (2 mM), tetraethylammonium-Cl (10 mM), $CdCl_2$ (50 μM), and nimodipine (1 μM) were added to the recording solution to reduce contamination from non-LVA T-type Ca^{2+} channel currents. The liquid junction potential for voltage-clamp solutions was calculated as +9.7 mV and corrected online. To construct a concentration-dependent response curve, we superfused the cells with Z944 after stable baseline recording. Percentage block of T-type Ca^{2+} channel current was calculated, and pooled data were plotted on a log scale and fitted with a Hill equation (Eq. 5), where y = fraction of binding sites filled, K_d = dissociation constant, L = ligand concentration, and n = Hill coefficient.

$$y = \left(\frac{L^n}{K_d + L^n}\right) \quad (5)$$

Current density for the HVA and LVA current was measured by applying 200-ms depolarizing test steps at 5-mV increments from −85 to 0 mV, from a holding potential of −90 mV. This protocol was repeated with a 50-ms depolarizing step to −20 mV preceding the test step, which removed the fast-inactivating LVA component, isolating the HVA component. The isolated HVA component was then subtracted from the HVA + LVA current recorded previously to isolate only the T-type Ca^{2+} current. This was then normalized to whole-cell capacitance to yield the current density. Currents recorded under voltage-clamp conditions were sampled at 20 kHz and filtered at 2.4 kHz, and leak current was subtracted with online P/5 subtraction.

Whole-cell current-clamp recordings were undertaken with fire-polished borosilicate glass pipettes (4 to 6 megohms) filled with the following solution containing 120 mM K-gluconate, 10 mM Hepes, 1 mM $MgCl_2$, 1 mM $CaCl_2$, 11 mM KCl, 11 mM EGTA, 4 mM MgATP, and 0.5 mM NaGTP (pH adjusted to 7.2 with KOH

and osmolarity adjusted to 290 mOsm/kg with D-mannitol). The liquid junction potential for current-clamp solutions was calculated as +13.3 mV and corrected off-line. To evaluate cell response to hyperpolarization and depolarization, we injected the current from −110 to +190 pA in 10-pA increments for a duration of 1.2 s at the cell's intrinsic RMP. Neurons that did not exhibit burst firing (as determined by a minimum of three action potentials within 150 ms of the current step) in response to depolarizing current steps were discarded. Voltage responses under current-clamp conditions were sampled at 50 kHz and filtered at 10 kHz.

Data analysis was performed with Clampfit 9 software and Origin version 7.5. Data followed a normal distribution, and statistical significance was calculated with one-way ANOVA with Tukey's post hoc test considering a P value of <0.05 as significant. Data were plotted as means ± SEM.

Evaluation of anti-seizure activity of Z941 and Z944 in GAERS

GAERS are a well-validated genetic rat model of GGE with absence seizures (*72*). The GAERS line was derived from a Wistar outbred rat strain and selected for spontaneous spike-and-wave activity. The strain used is fully inbred, and by 4 months of age, 100% of the animals express spontaneous absence seizures. The EEG brain wave recordings during the seizures in GAERS show generalized SWDs that have an abrupt onset and offset on a normal EEG background, closely resembling those seen during human absence seizures. During the seizures, which usually last from 5 to 30 s, behaviorally, the rats show arrest of activity and repetitive head nodding. The therapeutic profile of the seizures in GAERS is similar to that of human absences, being inhibited or exacerbated by similar antiepileptic drugs (*73*, *74*).

In vivo anti-seizure activity of Z941 and Z944 was assessed in eight female epileptic GAERS (180 to 250 g and 18 to 26 weeks) bred in the Ludwig Institute for Cancer Research, Melbourne, Australia. Rats were housed in separate cages in a temperature- and humidity-controlled room and allowed free access to rodent chow (WA stock feeders) and water under 12:12 light/dark conditions in the Biological Research Facility, Department of Medicine (Royal Melbourne Hospital), University of Melbourne. All experiments were approved by the Animal Ethics Committee of the University of Melbourne.

Rats were implanted with extradural recording electrodes, as previously described (*39*, *74*, *75*). Briefly, rats were anesthetized either by isoflurane (5% induction, 2.5 to 1.5% maintenance) in equal parts of medical air and oxygen or by intraperitoneal injection of a mixture of xylazine (10 mg/kg) and ketamine (75 mg/kg). Six burr holes were drilled into the skull, and gold-plated electrodes were implanted without breaching the dura. The electrodes were then held in place with dental cement (Vertex), and the rats were allowed to recover for 7 days before commencement of the experimental procedures.

Experiments were performed in a quiet, well-lit room in home cages. Wires were attached to the skull electrodes and connected to a computer running Compumedics ProFusion digital EEG acquisition software. EEG data were acquired at a sampling rate of 256 Hz without application of filters. After 60-min habituation, rats received intraperitoneal injections of drug, and after a further 15 min, the EEG was acquired for 120 min—the test period. Drug treatments were randomized, with at least 48 hours between treatments, and consisted of Z941 (10 or 30 mg/kg), Z944 (10 or 30 mg/kg), ethosuximide (100 mg/kg in 0.9% saline; Sigma), sodium valproate (200 mg/kg in 0.9% saline; Sigma), or the vehicle for Z941 and Z944 (10% DMSO in 0.5% carboxymethylcellulose). Over a 5-week period, each rat received all treatments (crossover design) in a randomized manner with a 48-hour washout period between dosing of test compound, control vehicle, and positive control articles. Each drug was coded such that the experimenter was blinded to the drug being administered.

Clinical observations of neurotoxic adverse effects were assessed every 15 min throughout the 120-min test period. These were quantified according to an ordinal scale of 0 to 4: 0, no sedation, normal movement; 1, slight sedation, slow movement but alert when startled; 2, mildly sedate, reduced struggle to restraint; 3, sedate, not moving in cage, but does respond to provocation; 4, very sedate, catatonic and unable to stand when provoked. The eight scores (taken for one experiment per rat) were then averaged, and group means were calculated for each treatment. Animals were also monitored daily for general health throughout the study period (that is, weight gain and fur condition).

SWDs were detected automatically with the Mighty EDF1 EEG viewing software (version 1.3.3), custom-designed to quantify seizures in GAERS, and subsequently manually checked by an investigator blinded to the treatment group of the animals. The following criteria were used: SWD burst of amplitude of more than three times baseline, a frequency of 6 to 12 Hz, and duration of longer than 0.5 s (*76*).The total percentage time spent in seizure activity, the average seizure duration, and the number of seizures were calculated for each experiment.

The cycle frequency of the SWDs (Hz) was analyzed for the highest dose of the Z941 (30 mg/kg) and Z944 (30 mg/kg) compared to the vehicle DMSO and ethosuximide treatments. The analysis was performed with Clampfit 10.2 software (Molecular Devices). For each rat for each of the four treatments, the frequency of SWD was measured by obtaining the average cycle frequency of the first 10 seizures during the 120-min target period. Note that for some traces, there were no seizures or fewer than 10 seizures during the entire 120-min period, so the average was obtained from a lesser number of seizures.

Evaluation of delta wave activity of Z944 in GAERS

Interictal EEG traces from GAERS receiving Z944 (10 mg/kg), ethosuximide (100 mg/kg), or vehicle intraperitoneally were analyzed for delta wave power with NeuroScan software (Compumedics). For this, the EEG recording for the first 45 min after the drug administration was selected. The 45-min block was then broken into 1-min intervals, which were analyzed with 2-s epochs. The epochs were manually reviewed, and any containing seizure activity or contaminated by artifact was excluded from the analysis. An FFT was applied to the remaining epochs, and the power for the delta activity (0 to 3.75 Hz) in each window was calculated. Any outliers, which were determined as points in which an individual value was greater than or less than twice the SD for the relevant band power, were removed from analysis.

Statistical analysis

Statistical analyses were performed with GraphPad Prism version 4.00 for Windows (GraphPad Software) using repeated-measures ANOVA and, if appropriate, Bonferroni post hoc tests with planned comparisons to compare between individual treatments. All data are expressed as means ± SEM, and differences were considered significant when $P < 0.05$.

SUPPLEMENTARY MATERIALS

www.sciencetranslationalmedicine.org/cgi/content/full/4/121/121ra19/DC1
Materials and Methods
Fig. S1. Concentration-dependent inhibition of recombinant T- and N-type Ca_V channel currents by Z944.

Fig. S2. Concentration-dependent inhibition of recombinant cardiac channel currents by Z944.
Fig. S3. Z944 does not affect the voltage dependence of $hCa_V3.2$ fast inactivation.
Fig. S4. Protocol used to measure the frequency dependence of Z944 inhibition of $hCa_V3.2$ currents.
Table S1. Effect of Z944 on action potentials in isolated rabbit cardiac Purkinje fibers.
Table S2. Evaluation of cardiovascular effects of Z944.
Table S3. Z994 does not alter the activation and deactivation kinetics of $hCa_V3.2$ channels.
Table S4. Z944 inhibition of $hCa_V3.2$ varied with frequency of stimulation.
References

REFERENCES AND NOTES

1. I. Mody, Ion channels in epilepsy. *Int. Rev. Neurobiol.* **42**, 199–226 (1998).
2. J. R. Hughes, Absence seizures: A review of recent reports with new concepts. *Epilepsy Behav.* **15**, 404–412 (2009).
3. E. Takahashi, K. Niimi, Modulators of voltage-dependent calcium channels for the treatment of nervous system diseases. *Recent Pat. CNS Drug Discov.* **4**, 96–111 (2009).
4. M. P. Jacobs, G. G. Leblanc, A. Brooks-Kayal, F. E. Jensen, D. H. Lowenstein, J. L. Noebels, D. D. Spencer, J. W. Swann, Curing epilepsy: Progress and future directions. *Epilepsy Behav.* **14**, 438–445 (2009).
5. G. W. Zamponi, P. Lory, E. Perez-Reyes, Role of voltage-gated calcium channels in epilepsy. *Pflugers Arch.* **460**, 395–403 (2010).
6. V. V. Bhise, G. D. Burack, D. E. Mandelbaum, Baseline cognition, behavior, and motor skills in children with new-onset, idiopathic epilepsy. *Dev. Med. Child Neurol.* **52**, 22–26 (2010).
7. P. J. Adams, T. P. Snutch, Calcium channelopathies: Voltage-gated calcium channels. *Subcell. Biochem.* **45**, 215–251 (2007).
8. W. A. Catterall, E. Perez-Reyes, T. P. Snutch, J. Striessnig, International Union of Pharmacology. XLVIII. Nomenclature and structure-function relationships of voltage-gated calcium channels. *Pharmacol. Rev.* **57**, 411–425 (2005).
9. E. M. Talley, L. L. Cribbs, J. H. Lee, A. Daud, E. Perez-Reyes, D. A. Bayliss, Differential distribution of three members of a gene family encoding low voltage-activated (T-type) calcium channels. *J. Neurosci.* **19**, 1895–1911 (1999).
10. L. Danober, C. Deransart, A. Depaulis, M. Vergnes, C. Marescaux, Pathophysiological mechanisms of genetic absence epilepsy in the rat. *Prog. Neurobiol.* **55**, 27–57 (1998).
11. D. Pinault, A. Slézia, L. Acsády, Corticothalamic 5–9 Hz oscillations are more pro-epileptogenic than sleep spindles in rats. *J. Physiol.* **574**, 209–227 (2006).
12. E. Tsakiridou, L. Bertollini, M. de Curtis, G. Avanzini, H. C. Pape, Selective increase in T-type calcium conductance of reticular thalamic neurons in a rat model of absence epilepsy. *J. Neurosci.* **15**, 3110–3117 (1995).
13. D. M. Porcello, S. D. Smith, J. R. Huguenard, Actions of U-92032, a T-type Ca^{2+} channel antagonist, support a functional linkage between I_T and slow intrathalamic rhythms. *J. Neurophysiol.* **89**, 177–185 (2003).
14. V. Crunelli, N. Leresche, Block of thalamic T-type Ca^{2+} channels by ethosuximide is not the whole story. *Epilepsy Curr.* **2**, 53–56 (2002).
15. J. C. Gomora, A. N. Daud, M. Weiergräber, E. Perez-Reyes, Block of cloned human T-type calcium channels by succinimide antiepileptic drugs. *Mol. Pharmacol.* **60**, 1121–1132 (2001).
16. M. Z. Gören, F. Onat, Ethosuximide: From bench to bedside. *CNS Drug Rev.* **13**, 224–239 (2007).
17. D. Kim, I. Song, S. Keum, T. Lee, M. J. Jeong, S. S. Kim, M. W. McEnery, H. S. Shin, Lack of the burst firing of thalamocortical relay neurons and resistance to absence seizures in mice lacking α_{1G} T-type Ca^{2+} channels. *Neuron* **31**, 35–45 (2001).
18. I. Song, D. Kim, S. Choi, M. Sun, Y. Kim, H. S. Shin, Role of the α1G T-type calcium channel in spontaneous absence seizures in mutant mice. *J. Neurosci.* **24**, 5249–5257 (2004).
19. W. L. Ernst, Y. Zhang, J. W. Yoo, S. J. Ernst, J. L. Noebels, Genetic enhancement of thalamocortical network activity by elevating α1G-mediated low-voltage-activated calcium current induces pure absence epilepsy. *J. Neurosci.* **29**, 1615–1625 (2009).
20. M. Vergnes, C. Marescaux, Cortical and thalamic lesions in rats with genetic absence epilepsy. *J. Neural Transm. Suppl.* **35**, 71–83 (1992).
21. K. L. Powell, S. M. Cain, C. Ng, S. Sirdesai, L. S. David, M. Kyi, E. Garcia, J. R. Tyson, C. A. Reid, M. Bahlo, S. J. Foote, T. P. Snutch, T. J. O'Brien, A $Ca_V3.2$ T-type calcium channel point mutation has splice-variant-specific effects on function and segregates with seizure expression in a polygenic rat model of absence epilepsy. *J. Neurosci.* **29**, 371–380 (2009).
22. Y. Chen, J. Lu, H. Pan, Y. Zhang, H. Wu, K. Xu, X. Liu, Y. Jiang, X. Bao, Z. Yao, K. Ding, W. H. Lo, B. Qiang, P. Chan, Y. Shen, X. Wu, Association between genetic variation of *CACNA1H* and childhood absence epilepsy. *Ann. Neurol.* **54**, 239–243 (2003).
23. S. E. Heron, H. Khosravani, D. Varela, C. Bladen, T. C. Williams, M. R. Newman, I. E. Scheffer, S. F. Berkovic, J. C. Mulley, G. W. Zamponi, Extended spectrum of idiopathic generalized epilepsies associated with *CACNA1H* functional variants. *Ann. Neurol.* **62**, 560–568 (2007).
24. J. Liang, Y. Zhang, J. Wang, H. Pan, H. Wu, K. Xu, X. Liu, Y. Jiang, Y. Shen, X. Wu, New variants in the *CACNA1H* gene identified in childhood absence epilepsy. *Neurosci. Lett.* **406**, 27–32 (2006).
25. J. Liang, Y. Zhang, Y. Chen, J. Wang, H. Pan, H. Wu, K. Xu, X. Liu, Y. Jiang, Y. Shen, X. Wu, Common polymorphisms in the *CACNA1H* gene associated with childhood absence epilepsy in Chinese Han population. *Ann. Hum. Genet.* **71**, 325–335 (2007).
26. B. Singh, A. Monteil, I. Bidaud, Y. Sugimoto, T. Suzuki, S. Hamano, H. Oguni, M. Osawa, M. E. Alonso, A. V. Delgado-Escueta, Y. Inoue, N. Yasui-Furukori, S. Kaneko, P. Lory, K. Yamakawa, Mutational analysis of *CACNA1G* in idiopathic generalized epilepsy. *Hum. Mutat.* **28**, 524–525 (2007).
27. H. Khosravani, C. Altier, B. Simms, K. S. Hamming, T. P. Snutch, J. Mezeyova, J. E. McRory, G. W. Zamponi, Gating effects of mutations in the $Ca_V3.2$ T-type calcium channel associated with childhood absence epilepsy. *J. Biol. Chem.* **279**, 9681–9684 (2004).
28. H. Khosravani, C. Bladen, D. B. Parker, T. P. Snutch, J. E. McRory, G. W. Zamponi, Effects of $Ca_V3.2$ channel mutations linked to idiopathic generalized epilepsy. *Ann. Neurol.* **57**, 745–749 (2005).
29. J. B. Peloquin, H. Khosravani, W. Barr, C. Bladen, R. Evans, J. Mezeyova, D. Parker, T. P. Snutch, J. E. McRory, G. W. Zamponi, Functional analysis of $Ca_V3.2$ T-type calcium channel mutations linked to childhood absence epilepsy. *Epilepsia* **47**, 655–658 (2006).
30. I. Vitko, Y. Chen, J. M. Arias, Y. Shen, X. R. Wu, E. Perez-Reyes, Functional characterization and neuronal modeling of the effects of childhood absence epilepsy variants of *CACNA1H*, a T-type calcium channel. *J. Neurosci.* **25**, 4844–4855 (2005).
31. I. Vitko, I. Bidaud, J. M. Arias, A. Mezghrani, P. Lory, E. Perez-Reyes, The I–II loop controls plasma membrane expression and gating of $Ca_V3.2$ T-type Ca^{2+} channels: A paradigm for childhood absence epilepsy mutations. *J. Neurosci.* **27**, 322–330 (2007).
32. T. A. Glauser, A. Cnaan, S. Shinnar, D. G. Hirtz, D. Dlugos, D. Masur, P. O. Clark, E. V. Capparelli, P. C. Adamson; Childhood Absence Epilepsy Study Group, Ethosuximide, valproic acid, and lamotrigine in childhood absence epilepsy. *N. Engl. J. Med.* **362**, 790–799 (2010).
33. T. P. Snutch, Targeting chronic and neuropathic pain: The N-type calcium channel comes of age. *NeuroRx* **2**, 662–670 (2005).
34. C. C. Kuo, R. S. Chen, L. Lu, R. C. Chen, Carbamazepine inhibition of neuronal Na^+ currents: Quantitative distinction from phenytoin and possible therapeutic implications. *Mol. Pharmacol.* **51**, 1077–1083 (1997).
35. C. C. Kuo, B. P. Bean, Slow binding of phenytoin to inactivated sodium channels in rat hippocampal neurons. *Mol. Pharmacol.* **46**, 716–725 (1994).
36. C. C. Kuo, L. Lu, Characterization of lamotrigine inhibition of Na^+ channels in rat hippocampal neurones. *Br. J. Pharmacol.* **121**, 1231–1238 (1997).
37. G. W. Zamponi, Z. P. Feng, L. Zhang, H. Pajouhesh, Y. Ding, F. Belardetti, H. Pajouhesh, D. Dolphin, L. A. Mitscher, T. P. Snutch, Scaffold-based design and synthesis of potent N-type calcium channel blockers. *Bioorg. Med. Chem. Lett.* **19**, 6467–6472 (2009).
38. C. Marescaux, M. Vergnes, A. Depaulis, Genetic absence epilepsy in rats from Strasbourg—A review. *J. Neural Transm. Suppl.* **35**, 37–69 (1992).
39. M. J. Morris, E. Gannan, L. M. Stroud, A. G. Beck-Sickinger, T. J. O'Brien, Neuropeptide Y suppresses absence seizures in a genetic rat model primarily through effects on Y receptors. *Eur. J. Neurosci.* **25**, 1136–1143 (2007).
40. L. M. Stroud, T. J. O'Brien, B. Jupp, C. Wallengren, M. J. Morris, Neuropeptide Y suppresses absence seizures in a genetic rat model. *Brain Res.* **1033**, 151–156 (2005).
41. T. Zheng, A. L. Clarke, M. J. Morris, C. A. Reid, S. Petrou, T. J. O'Brien, Oxcarbazepine, not its active metabolite, potentiates $GABA_A$ activation and aggravates absence seizures. *Epilepsia* **50**, 83–87 (2009).
42. E. M. Talley, G. Solórzano, A. Depaulis, E. Perez-Reyes, D. A. Bayliss, Low-voltage-activated calcium channel subunit expression in a genetic model of absence epilepsy in the rat. *Brain Res. Mol. Brain Res.* **75**, 159–165 (2000).
43. J. R. Huguenard, D. A. Prince, A novel T-type current underlies prolonged Ca^{2+}-dependent burst firing in GABAergic neurons of rat thalamic reticular nucleus. *J. Neurosci.* **12**, 3804–3817 (1992).
44. P. M. Joksovic, D. A. Bayliss, S. M. Todorovic, Different kinetic properties of two T-type Ca^{2+} currents of rat reticular thalamic neurones and their modulation by enflurane. *J. Physiol.* **566**, 125–142 (2005).
45. P. M. Joksovic, B. C. Brimelow, J. Murbartián, E. Perez-Reyes, S. M. Todorovic, Contrasting anesthetic sensitivities of T-type Ca^{2+} channels of reticular thalamic neurons and recombinant $Ca_V3.3$ channels. *Br. J. Pharmacol.* **144**, 59–70 (2005).
46. P. M. Joksovic, M. T. Nelson, V. Jevtovic-Todorovic, M. K. Patel, E. Perez-Reyes, K. P. Campbell, C. C. Chen, S. M. Todorovic, $Ca_V3.2$ is the major molecular substrate for redox regulation of T-type Ca^{2+} channels in the rat and mouse thalamus. *J. Physiol.* **574**, 415–430 (2006).
47. D. Contreras, The role of T-channels in the generation of thalamocortical rhythms. *CNS Neurol. Disord. Drug Targets* **5**, 571–585 (2006).
48. A. Destexhe, T. J. Sejnowski, The initiation of bursts in thalamic neurons and the cortical control of thalamic sensitivity. *Philos. Trans. R. Soc. Lond. B Biol. Sci.* **357**, 1649–1657 (2002).
49. D. A. Coulter, J. R. Huguenard, D. A. Prince, Calcium currents in rat thalamocortical relay neurones: Kinetic properties of the transient, low-threshold current. *J. Physiol.* **414**, 587–604 (1989).

50. E. de la Peña, E. Geijo-Barrientos, Laminar localization, morphology, and physiological properties of pyramidal neurons that have the low-threshold calcium current in the guinea-pig medial frontal cortex. *J. Neurosci.* **16**, 5301–5311 (1996).
51. M. Deschênes, M. Paradis, J. P. Roy, M. Steriade, Electrophysiology of neurons of lateral thalamic nuclei in cat: Resting properties and burst discharges. *J. Neurophysiol.* **51**, 1196–1219 (1984).
52. H. Jahnsen, R. Llinás, Ionic basis for the electro-responsiveness and oscillatory properties of guinea-pig thalamic neurones in vitro. *J. Physiol.* **349**, 227–247 (1984).
53. R. Llinás, H. Jahnsen, Electrophysiology of mammalian thalamic neurones in vitro. *Nature* **297**, 406–408 (1982).
54. A. L. Sherwin, Ethosuximide: Clinical use, in *Antiepileptic Drugs* (Raven Press, New York, 1989), pp. 685–689.
55. J. P. Manning, D. A. Richards, N. Leresche, V. Crunelli, N. G. Bowery, Cortical-area specific block of genetically determined absence seizures by ethosuximide. *Neuroscience* **123**, 5–9 (2004).
56. D. A. Richards, J. P. Manning, D. Barnes, L. Rombola, N. G. Bowery, S. Caccia, N. Leresche, V. Crunelli, Targeting thalamic nuclei is not sufficient for the full anti-absence action of ethosuximide in a rat model of absence epilepsy. *Epilepsy Res.* **54**, 97–107 (2003).
57. T. Broicher, T. Seidenbecher, P. Meuth, T. Munsch, S. G. Meuth, T. Kanyshkova, H. C. Pape, T. Budde, T-current related effects of antiepileptic drugs and a Ca^{2+} channel antagonist on thalamic relay and local circuit interneurons in a rat model of absence epilepsy. *Neuropharmacology* **53**, 431–446 (2007).
58. H. K. Meeren, J. P. Pijn, E. L. Van Luijtelaar, A. M. Coenen, F. H. Lopes da Silva, Cortical focus drives widespread corticothalamic networks during spontaneous absence seizures in rats. *J. Neurosci.* **22**, 1480–1495 (2002).
59. D. Pinault, Cellular interactions in the rat somatosensory thalamocortical system during normal and epileptic 5–9 Hz oscillations. *J. Physiol.* **552**, 881–905 (2003).
60. P. O. Polack, I. Guillemain, E. Hu, C. Deransart, A. Depaulis, S. Charpier, Deep layer somatosensory cortical neurons initiate spike-and-wave discharges in a genetic model of absence seizures. *J. Neurosci.* **27**, 6590–6599 (2007).
61. L. R. Silva, Y. Amitai, B. W. Connors, Intrinsic oscillations of neocortex generated by layer 5 pyramidal neurons. *Science* **251**, 432–435 (1991).
62. Z. Q. Yang, J. C. Barrow, W. D. Shipe, K. A. Schlegel, Y. Shu, F. V. Yang, C. W. Lindsley, K. E. Rittle, M. G. Bock, G. D. Hartman, V. N. Uebele, C. E. Nuss, S. V. Fox, R. L. Kraus, S. M. Doran, T. M. Connolly, C. Tang, J. E. Ballard, Y. Kuo, E. D. Adarayan, T. Prueksaritanont, M. M. Zrada, M. J. Marino, V. K. Graufelds, A. G. DiLella, I. J. Reynolds, H. M. Vargas, P. B. Bunting, R. F. Woltmann, M. M. Magee, K. S. Koblan, J. J. Renger, Discovery of 1,4-substituted piperidines as potent and selective inhibitors of T-type calcium channels. *J. Med. Chem.* **51**, 6471–6477 (2008).
63. S. S. Nahm, K. Y. Jung, M. K. Enger, W. H. Griffith, L. C. Abbott, Differential expression of T-type calcium channels in P/Q-type calcium channel mutant mice with ataxia and absence epilepsy. *J. Neurobiol.* **62**, 352–360 (2005).
64. Y. Zhang, M. Mori, D. L. Burgess, J. L. Noebels, Mutations in high-voltage-activated calcium channel genes stimulate low-voltage-activated currents in mouse thalamic relay neurons. *J. Neurosci.* **22**, 6362–6371 (2002).
65. B. Terzioğlu, C. Aypak, F. Y. Onat, E. Küçükibrahimoğlu, A. E. Ozkaynakçi, M. Z. Goren, The effects of ethosuximide on amino acids in genetic absence epilepsy rat model. *J. Pharmacol. Sci.* **100**, 227–233 (2006).
66. J. Lee, D. Kim, H. S. Shin, Lack of delta waves and sleep disturbances during non-rapid eye movement sleep in mice lacking $\alpha 1_G$-subunit of T-type calcium channels. *Proc. Natl. Acad. Sci. U.S.A.* **101**, 18195–18199 (2004).
67. M. P. Anderson, T. Mochizuki, J. Xie, W. Fischler, J. P. Manger, E. M. Talley, T. E. Scammell, S. Tonegawa, Thalamic $Ca_v3.1$ T-type Ca^{2+} channel plays a crucial role in stabilizing sleep. *Proc. Natl. Acad. Sci. U.S.A.* **102**, 1743–1748 (2005).
68. R. L. Kraus, Y. Li, Y. Gregan, A. L. Gotter, V. N. Uebele, S. V. Fox, S. M. Doran, J. C. Barrow, Z. Q. Yang, T. S. Reger, K. S. Koblan, J. J. Renger, In vitro characterization of T-type calcium channel antagonist TTA-A2 and in vivo effects on arousal in mice. *J. Pharmacol. Exp. Ther.* **335**, 409–417 (2010).
69. G. C. Faas, M. Vreugdenhil, W. J. Wadman, Calcium currents in pyramidal CA1 neurons in vitro after kindling epileptogenesis in the hippocampus of the rat. *Neuroscience* **75**, 57–67 (1996).
70. H. Su, D. Sochivko, A. Becker, J. Chen, Y. Jiang, Y. Yaari, H. Beck, Upregulation of a T-type Ca^{2+} channel causes a long-lasting modification of neuronal firing mode after status epilepticus. *J. Neurosci.* **22**, 3645–3655 (2002).
71. M. E. Hildebrand, T. P. Snutch, Contributions of T-type calcium channels to the pathophysiology of pain signaling. *Drug Discov. Today Dis. Mech.* **3**, 335–341 (2006).
72. C. Marescaux, M. Vergnes, G. Micheletti, A. Depaulis, J. Reis, L. Rumbach, J. M. Warter, D. Kurtz, A genetic form of petit mal absence in Wistar rats. *Rev. Neurol.* **140**, 63–66 (1984).
73. C. Marescaux, M. Vergnes, Genetic Absence Epilepsy in Rats from Strasbourg (GAERS). *Ital. J. Neurol. Sci.* **16**, 113–118 (1995).
74. L. Liu, T. Zheng, M. J. Morris, C. Wallengren, A. L. Clarke, C. A. Reid, S. Petrou, T. J. O'Brien, The mechanism of carbamazepine aggravation of absence seizures. *J. Pharmacol. Exp. Ther.* **319**, 790–798 (2006).
75. N. C. Jones, M. R. Salzberg, G. Kumar, A. Couper, M. J. Morris, T. J. O'Brien, Elevated anxiety and depressive-like behavior in a rat model of genetic generalized epilepsy suggesting common causation. *Exp. Neurol.* **209**, 254–260 (2008).
76. C. Marescaux, M. Vergnes, R. Bernasconi, GABAB receptor antagonists: Potential new anti-absence drugs. *J. Neural Transm. Suppl.* **35**, 179–188 (1992).

Acknowledgments: The monkey cardiovascular telemetry experiments were performed by Charles River, and the rabbit Purkinje fiber experiments were performed by ChanTest. **Funding:** Supported by an operating grant from the Canadian Institutes of Health Research (#10677) and a Canada Research Chair in Biotechnology and Genomics-Neurobiology (T.P.S.), BC Epilepsy Society/Michael Smith Foundation for Health Research Trainee Award (S.M.C.), and Australian NH&MRC Project grant #628723 (T.J.O. and K.L.P.). **Author contributions:** FLIPR data were obtained by K.K. and J.-L.M. Stable cell lines expressing voltage-gated ion channels were generated by J.M. and D.P. Electrophysiological recordings on recombinant voltage-gated channels were performed by E.T., M.W., C.E., X.J., and P.S. Electrophysiological recordings from thalamic neurons and slices were performed by S.M.C. The monkey cardiovascular telemetry and rabbit Purkinje fiber data were monitored by M.F.-M. Synthesis of Z944 and Z941 was directed by H.P. EEG data were obtained and analyzed by G.R., E.B., N.C.J., and K.L.P. M.P. oversaw the preclinical aspects of Z944 development. T.J.O. directed the in vivo epilepsy research on GAERS. T.P.S. contributed to the T-type blocker rational design and also directed aspects of the research related to assay development, compound screening, biophysical characterizations, and preclinical development. E.T. drafted the manuscript, and T.J.O., K.L.P., N.C.J., S.M.C., and T.P.S. edited various subsequent versions. **Competing interests:** E.T., J.M., C.E., P.S., J.-L.M., D.P., M.F.-M., M.P., H.P., and T.P.S. are either current or former employees of Zalicus Pharmaceuticals Ltd. (a subsidiary of Zalicus Inc.) and own stock and/or have been granted stock options. Zalicus Pharmaceuticals (formerly Neuromed Pharmaceuticals) holds a patent for Z941 and Z944 (*N*-piperidinyl acetamide derivatives as calcium channel blockers; WO 2009146540-1).

Submitted 24 August 2011
Accepted 18 January 2012
Published 15 February 2012
10.1126/scitranslmed.3003120

Citation: E. Tringham, K. L. Powell, S. M. Cain, K. Kuplast, J. Mezeyova, M. Weerapura, C. Eduljee, X. Jiang, P. Smith, J.-L. Morrison, N. C. Jones, E. Braine, G. Rind, M. Fee-Maki, D. Parker, H. Pajouhesh, M. Parmar, T. J. O'Brien, T. P. Snutch, T-type calcium channel blockers that attenuate thalamic burst firing and suppress absence seizures. *Sci. Transl. Med.* **4**, 121ra19 (2012).